Geophysical Journal International

Local site-effects for the city of Thessaloniki (N. Greece) using a 3-D finite-difference method: a case of complex dependence on source and model parameters

A. A. Skarlatoudis,[1] C. B. Papazachos,[1] N. Theodoulidis,[2] J. Kristek[3] and P. Moczo[3]

[1]*Department of Geology, University of Thessaloniki, Thessaloniki, Greece, E-mail: askarlat@geo.auth.gr*
[2]*Institute of Engineering Seismology and Earthquake Engineering, ITSAK, Greece*
[3]*Department of Astronomy, Physics of the Earth and Meteorology, Comenius University, Bratislava, Slovak Republic*

SUMMARY
The site effects of seismic motion in the metropolitan area of the city of Thessaloniki (Northern Greece) are investigated using a 3-D finite-difference modelling approach. Three different seismic scenarios are assumed with two different focal mechanisms for each one. Standard spectral ratios (SSR) are calculated from 3-D synthetics and compared with the ratios from the recorded motion, as well as ratios obtained from 1-D and 2-D modelling by other researchers. The average SSR curves from the six scenarios are in good agreement with the empirical ones, whereas the SSR results from 3-D modelling are different from those from 1-D modelling, exhibiting higher fundamental frequencies and larger amplification amplitudes, in much better agreement with observed SSR ratios. Comparisons of Fourier amplitude spectra obtained for various scenarios for the broader area of Thessaloniki show considerable dependence of the site effects on the source properties (position, depth and fault-plane solution), as well as on the local structure.

Key words: Earthquake ground motions; Site effects; Wave propagation.

1 INTRODUCTION

The city of Thessaloniki (Northern Greece) is located in the Axios-Vardar geological zone, which is adjacent to the Servomacedonian massif, one of the most seismotectonically active regions in Europe (Papazachos *et al.* 1983) (Fig. 1). The seismotectonic setting of the broader area (Servomacedonian massif) is characterized mostly by normal faults with an E–W strike due to the extensive stress field, with a more or less N–S direction, as well as secondary, mainly SE–NW, striking faults (Vamvakaris *et al.* 2006).

Fig. (2a) shows a general overview of the geological structure of the broader study area. Thessaloniki with its suburbs lies across the Thermaikos gulf and is situated on three main large-scale geological formations, oriented in an NW–SE direction, following the well-known local Alpine trending of continental-type basins and grabens in this area. The deepest bedrock formation consists of gneiss, epigneiss and green schists, with outcroping manifestation at the N-NE borders of the urban area (dark grey areas in Figs 2a and b). These crystalline rocks constitute the bedrock basement, with a depth >400 m near the coastline, whereas its depth is continuously increasing towards the centre of the Thermaikos gulf, where the Neogene sediments exceed the thickness of 2500 m (Fig. 2a).

Above this basement, the basin has been filled by sedimentary deposits, mainly of the Neogene and Quaternary period (medium and light grey areas in Fig. 2b, respectively). These geological for-

mations are dominated by the local red silty clay series, which cover the bedrock basement beneath the city. Finally, the topmost surface layer consists mainly of recent deposits of Holocene clays, sands and pebbles.

The city has suffered large earthquakes throughout its history (Fig. 1) and many of them caused significant damage and human losses (Papazachos & Papazachou 2002). Thessaloniki was the first big modern city in Greece which was hit by a destructive earthquake (20 June 1978, $M_{6.5}$), attracting several researchers to perform microzonation studies, as well as to quantify site effects and predict structural behaviour during strong earthquakes (e.g. Sherif, 1973; Kobayashi 1974; Leventakis & Roussopoulos 1974; Pitilakis *et al.* 1982; Tsotsos & Zissis-Tegos 1986; Chávez-García *et al.* 1990; Lachet *et al.* 1996; Panou *et al.* 2005; Triantafyllidis *et al.* 1998, 1999, 2004a,b; Raptakis *et al.* 1998, 2004a,b).

The first effort that led to the construction of a detailed 3-D geophysical/geotechnical model for the sedimentary formations and bedrock geometry of the city of Thessaloniki (model AN01 hereinafter) was performed by Anastasiadis *et al.* (2001), who studied the 1-D geometry and the dynamic properties of major soil formations of the metropolitan area of Thessaloniki using a large number of borehole data and laboratory measurements. The second major effort was conducted by Apostolidis *et al.* (2004a,b) (model AP04 hereinafter), who performed array ambient noise measurements for 16 sites in the broader area of Thessaloniki using the SPAC
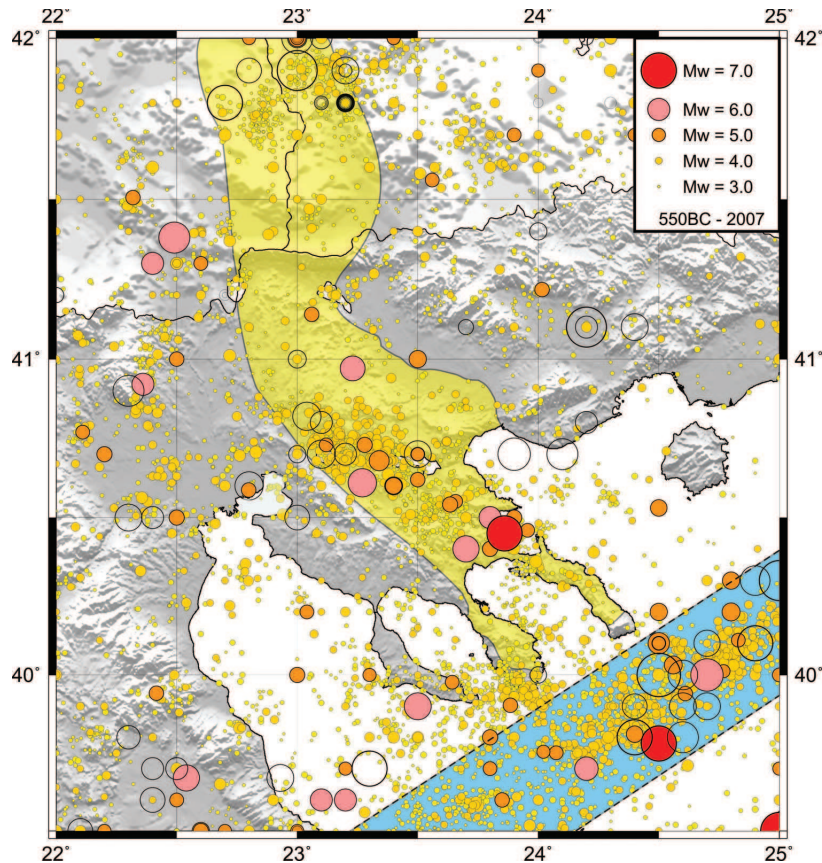
GJI Seismology

Figure 1. Map of known earthquakes with $M \geq 3.0$ which occurred in the broader area of central-northern Greece from the historical times (550 BC) til 2007. Open circles denote epicentres of historical earthquakes (before 1911). Two areas of high seismicity level can be identified, namely the Servomacedonian massif (yellow area) and the North Aegean Trough (blue area).

technique. The 1-D V_s-profiles determined from the inversion of noise dispersion curves for these sites together with the available geotechnical data (mainly from the AN01 model) were used to derive a revised 3-D geophysical model for the study area.

In this study the finite-difference (FD) method was used to numerically simulate the site response for 11 selected sites of the metropolitan area of Thessaloniki for which earthquake recordings were also available. Theoretical standard spectral ratios (SSR) are compared with those obtained from the recorded motions, whereas SSR and Fourier amplitude spectra (FAS) are used to evaluate the variability of ground motion due to 3-D soil response as well as different seismic excitation. As a result, the study does not include any time-domain comparisons but focuses on the validation of the available models in the frequency domain using the available empirical transfer functions for selected sites, to quantify the effect of various factors (3-D model and its uncertainties, source location, focal mechanisms, etc.) in the final FD synthetics.

2 GEOLOGICAL MODEL

For the model selection, preliminary tests were initially performed for the more recent AP04 model. However, this model was based in a 'reverse' approach, where after estimating the V_P and V_S depth variation for the sites where ambient noise measurements were performed, soil formations were determined for the whole study area on the basis of arbitrary V_S velocity intervals. This approach re-

sulted in the introduction of 'artificial' model layers (corresponding to specific V_S-velocity intervals) and not to layers that correspond to real geological sedimentary formations, which are better described by the relatively older available model (AN01).

To test the effect of this model generation approach on the performance of the AP04 model for FD simulations, a large number of synthetics was computed for the 11 selected sites. Comparisons with empirical transfer functions for most of the sites studied showed a relatively poor performance. This behaviour is probably due to the specific velocity averaging and grouping adopted in the AP04 model, hence results for this model were not further examined and only the AN01 model was employed in this study.

Since the AN01 model covers a part of the metropolitan area of Thessaloniki (Fig. 2b), it was extended within the dashed-line area shown in Fig. (2b) using the general geometry (but not the corresponding grouped velocity values) of the main formations, as provided by the AP04 model (the original coverage of the AN01 and AP04 models is also shown in Fig. 2b). This extrapolation mainly concerns areas for which information on the geometry and properties of geological formations was not available for the AN01 model (mainly the northwestern and southeastern part of the model, see Fig. 2b).

For the northeastern part of the model the dominating formation is the bedrock (mainly gneiss), with surface manifestation throughout the largest part of this area (Fig. 2b). The AN01 model was also extrapolated towards this direction, adopting the presence of the bedrock formation for the whole NE area of the computational
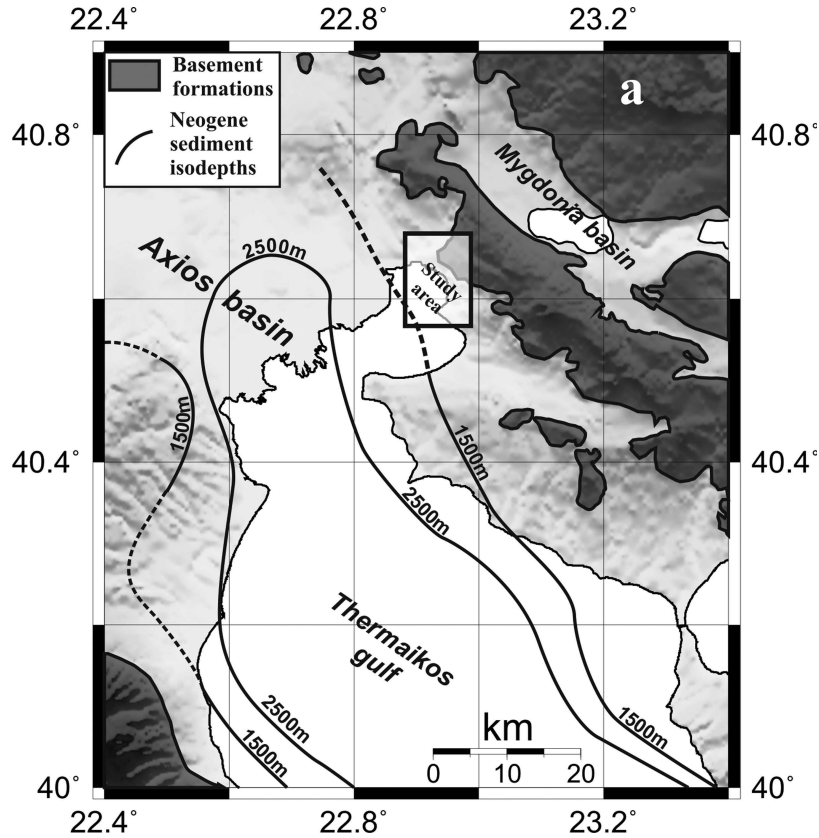
Figure 2. (a) Map of the broader study area, showing the general geological features of the Axios Basin and Thermaikos Gulf. Neogene sediments isodepth lines (Lalechos & Savoyat 1979) together with basement formations (dark areas in the map) are also shown. (b) Map showing the major soil formations in the study area (broader area of the city of Thessaloniki). The bedrock formation is denoted with the dark-grey shade, while with the medium and light grey shades correspond to the Neogene and Quarternary formations, respectively. The larger (square) hatched area represents the original coverage of Apostolidis *et al.*'s (2004b) geophysical/geotechnical model (AP04), while the smaller (oblique) one is the corresponding coverage of the Anastasiadis *et al.* (2001) geophysical/geotechnical model (AN01). The white dashed line corresponds to the limits of the modified AN01 model (see also Fig. 3). The cross-section LEP-OBS is also shown together with the corresponding structure of the model formations.

model. Furthermore, for the southwestern part of the model (sea area), where the bedrock depth attains large values and the total sedimentary cover becomes very thick, all layers were arbitrarily extended and thickened. The typical structure of the model formations along a cross-section connecting two of the sites studied (LEP-OBS) with a NE–SW direction and located in the centre of the model is also shown in Fig. (2b), and clearly verifies the gradual sediment thickening in this direction. Despite the fact that accurate information for the sea area does not exist, larger scale studies have identified the continuous thickening of Cenozoic sedimentary formations towards the central part of the Thermaikos gulf, several tens of kilometres to the southwest of the city of Thessaloniki (Lalechos & Savoyat 1979; Roussos 1994). The continuous thickening of the sedimentary formations towards the W–SW direction is clearly delineated by the Neogene sediments thickness lines from Lalechos & Savoyat (1979) presented in Fig. 2a. Taking this into account, the proposed extrapolation approach should have practically no impact on the modelling results, as in all examined scenarios in this study the earthquakes were located to the North, Northeast and East of Thessaloniki, where most of the large events of the high seismicity Servomacedonian massif occur (Fig. 1). Therefore, seismic waves do not propagate in this SW part of the model before reaching the city of Thessaloniki and significant backscattering and reflecting energy is not expected from the sea area due to the general gradual increase of the sedimentary layer thickness and the associated

bedrock depth. Fig. 3 shows the depth variations of the different soil formations of the modified AN01 model, covering an area of 9×12 km^2, after the procedure previously described.

3 NUMERICAL-SIMULATION METHOD

For numerical simulations an explicit 3-D fourth-order velocity-stress FD scheme was used. The scheme solves the equation of motion and Hooke's law for viscoelastic medium with rheology of the generalized Maxwell body,

$$\rho \dot{v}_i = \sigma_{ij,j} + f_i \tag{1}$$

and

$$\dot{\sigma}_{ij} = \kappa \dot{\varepsilon}_{kk} \delta_{ij} + 2\mu \left(\dot{\varepsilon}_{ij} - \frac{1}{3} \dot{\varepsilon}_{kk} \delta_{ij} \right)$$
$$- \sum_{l}^{4} \left[\kappa Y_l^\kappa \xi_l^{kk} \delta_{ij} + 2\mu Y_l^\mu \left(\xi_l^{ij} - \frac{1}{3} \xi_l^{kk} \delta_{ij} \right) \right], \tag{2}$$

$$\dot{\xi}_l^{ij} + \omega_l \xi_l^{ij} = \omega_l \dot{\varepsilon}_{ij}; \quad l = 1, \dots, 4. \tag{3}$$

Let (x_1, x_2, x_3) be Cartesian coordinates. Then $\rho(x_i); i \in \{1, 2, 3\}$, is density, $\kappa(x_i)$ and $\mu(x_i)$ are unrelaxed (elastic) bulk and shear moduli, $Y_l^\kappa(x_i, \omega_l)$ and $Y_l^\mu(x_i, \omega_l)$ anelastic coefficients, ω_l lth angular relaxation frequency, $\vec{v}(x_i, t)$ particle-velocity vector, t time,
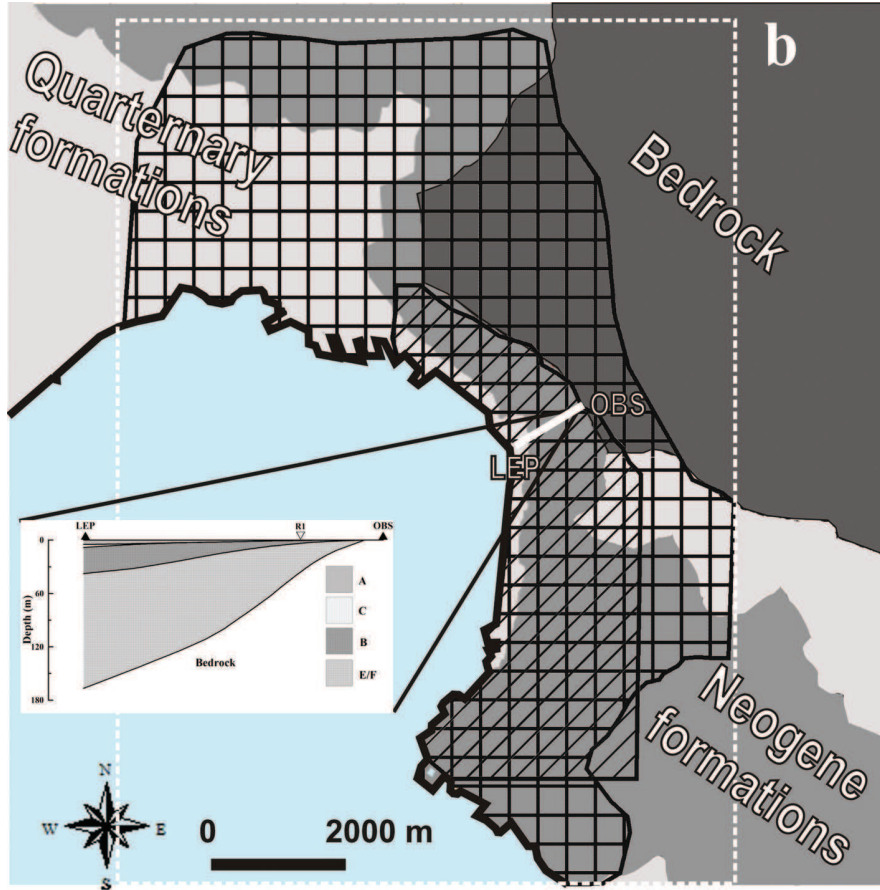
Figure 2. (*Continued.*)

$\vec{f}(x_i, t)$ body force per unit volume, $\sigma_{ij}(x_k, t)$ and $\varepsilon_{ij}(x_k, t)$; $i, j, k \in \{1, 2, 3\}$ stress and strain tensors, $\xi_l^{ij}(x_k, t; \omega_l)$ material-independent anelastic functions. Summation convention does not apply to index l. The anelastic coefficients are obtained from

$$Y_l^\kappa = \left(\alpha^2 Y_l^\alpha - \frac{4}{3}\beta^2 Y_l^\beta\right) \Big/ \left(\alpha^2 - \frac{4}{3}\beta^2\right),$$
$$Y_l^\mu = Y_l^\beta; \quad l = 1, \ldots, 4 \tag{4}$$

where α and β are elastic (corresponding to the unrelaxed moduli) *P*- and *S*-wave velocities, and anelastic coefficients $Y_l^\alpha(\omega_l)$ and $Y_l^\beta(\omega_l)$ are obtained from the desired or measured quality factor values at frequencies $\tilde{\omega}_k$

$$Q_\nu^{-1}(\tilde{\omega}_k) = \sum_{l=1}^{n} \frac{\omega_l \tilde{\omega}_k + \omega_l^2 Q_\nu^{-1}(\tilde{\omega}_k)}{\omega_l^2 + \tilde{\omega}_k^2} Y_l^\nu(\omega_l);$$
$$k = 1, \ldots, 7, \quad \nu \in \{\alpha, \beta\}. \tag{5}$$

The FD scheme sufficiently accurately accounts for the geometry of the material interfaces. The schemes for solving the equation of motion and time derivative of Hooke's law have the same structure as standard fourth-order velocity staggered-grid schemes. The accuracy of the scheme with respect to the material interfaces is due to the definition of the effective material grid parameters. The effective grid density for a corresponding particle velocity component is evaluated as an integral volume arithmetic average of density inside a grid cell centered at the grid position of the corresponding particle velocity component; for example density at the grid

position $I, J + 1/2, K + 1/2$ is defined by

$$\rho_{I,J+1/2,K+1/2}^A = \frac{1}{h^3} \int_{x_{I-1/2}}^{x_{I+1/2}} \int_{y_J}^{y_{J+1}} \int_{z_K}^{z_{K+1}} \rho \, dx \, dy \, dz. \tag{6}$$

The effective grid unrelaxed bulk and shear moduli are evaluated as integral volume harmonic averages of moduli in respective grid cells, centered at grid positions of the stress-tensor components; for example

$$\kappa_{I+1/2,J+1/2,K+1/2}^H = \left[\frac{1}{h^3} \int_{x_I}^{x_{I+1}} \int_{y_J}^{y_{J+1}} \int_{z_K}^{z_{K+1}} \frac{1}{\kappa} \, dx \, dy \, dz\right]^{-1}. \tag{7}$$

The integrals are evaluated numerically and the grid cell can contain a material discontinuity. The material parameterization enables the FD scheme to sense the true position of the material interfaces, even within a grid cell. The anelastic coefficients Y_l^κ and Y_l^μ are determined as follows: An average viscoelastic modulus in the frequency domain is numerically determined for a cell as an integral harmonic average. A corresponding quality factor is then determined from the averaged viscoelastic modulus at specified frequencies. Eq. (5) for the bulk and shear moduli are then used to determine average anelastic functions. A coarse spatial distribution of the anelastic functions is applied to reduce the memory requirements. For more on the scheme for interior gridpoints and material parameterization see Moczo *et al.* (2002) and Kristek & Moczo (2003). For a comprehensive exposition see monograph by Moczo *et al.* (2007).

Adjusted fourth-order accurate FD approximations are applied at the planar free surface (Kristek *et al.* 2002). The unsplit PML
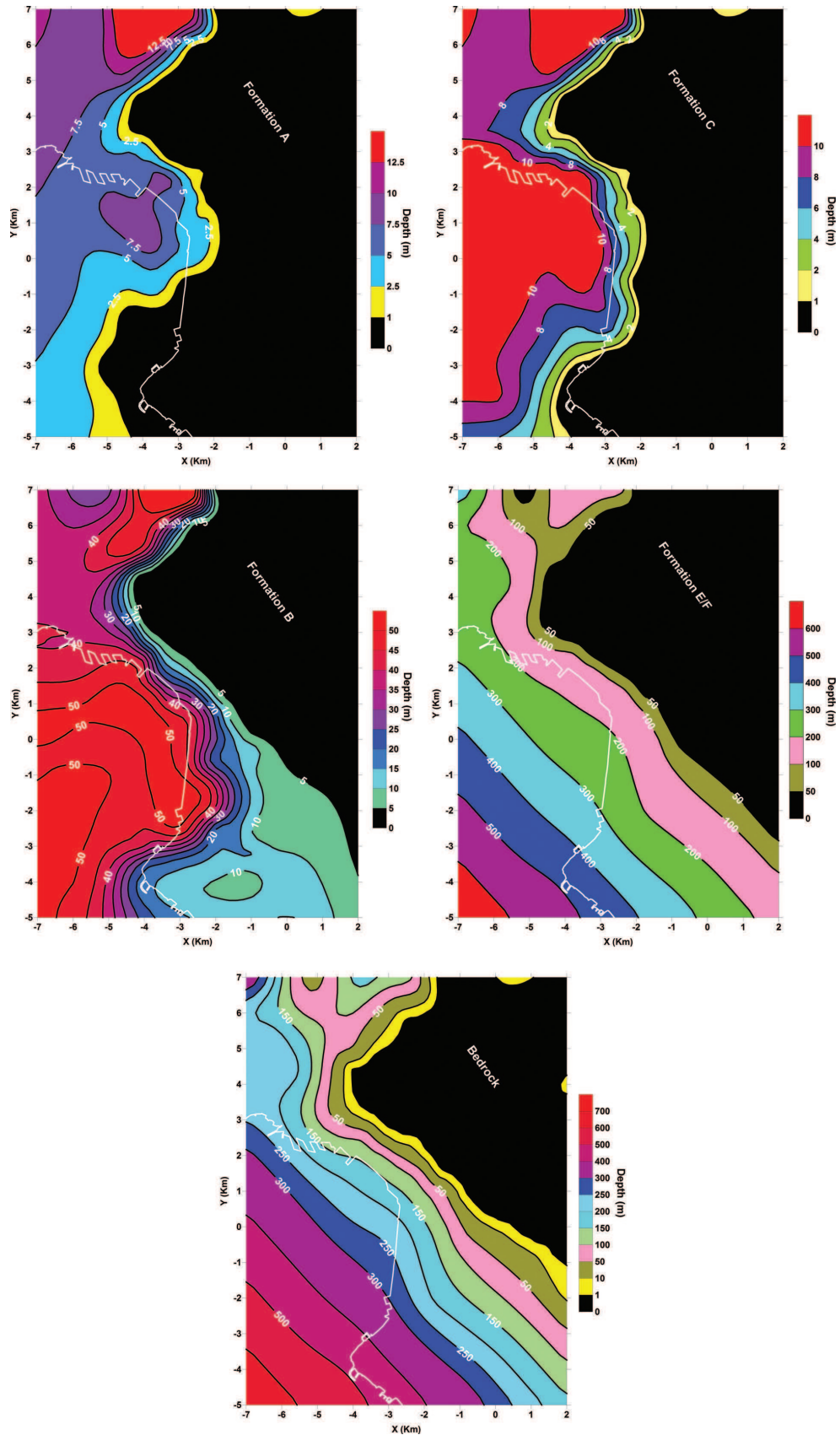
Figure 3. Depth and geometry of the soil formations of the modified AN01 geophysical/geotechnical model. The coastline is depicted with a white solid line. The area covered corresponds to the extrapolated AN01 geophysical/geotechnical model (see text for details).

formulation is used to prevent spurious reflections from the boundaries of the grid (Skarlatoudis *et al.* 2006; Kristek *et al.* 2009a).

It is advantageous to cover surface sediments with lower seismic wave velocities by a fine spatial grid and underlying stiffer bedrock with larger velocities by a coarser spatial grid: the number of gridpoints and consequently the computer memory and time requirements are significantly reduced compared to the uniform grid. To make such a combined (or discontinuous) spatial grid efficient, the ratio of the size of the spatial grid spacing in the coarser grid and that in the finer grid should correspond to the ratio of the shear wave velocities in the stiffer bedrock and softer sediments. Moczo *et al.* (2007) and Kristek *et al.* (2009b) present a discontinuous spatial grid that allows choosing the ratio (an odd number) of the spatial grid spacings in the coarser and finer grids.

4 COMPUTATIONAL MODEL

The true model geometry of the material interfaces as well as the smooth material heterogeneity inside the sedimentary body are accounted for in the evaluation of the effective material elastic and anelastic grid parameters using relations (4)–(7) and the approach described therein. As previously noted the scheme using the integral volume harmonic averages of the moduli and integral volume arithmetic average of density, evaluated for each cell centered at a relevant grid position, is capable to sense the true position of the material interfaces within the grid cell.

The constant $Q(\omega)$ law is simulated using the rheology of the generalized Maxwell body. The so-called coarse grid graining is applied in the spatial discretization of the anelastic coefficients and functions. Since for the existing models Q_α values were not available, they were estimated using the relation

$$\frac{1}{Q_\alpha} = \frac{4}{3} \left(\frac{\beta^2}{\alpha^2} \right) \frac{1}{Q_\beta}. \tag{8}$$

Values of the material parameters in each formation in the adopted model, Fig. 3, are listed in Table 1.

For all computations, the adopted approach requires that the computational model must include the hypocenters of the earthquakes to be modelled, thus, the modified AN01 geophysical/geotechnical model (Fig. 3) should be sufficiently large to meet this condition. As previously mentioned, the modelled earthquake hypocenters in this study were located to the North, Northeast and East of Thessaloniki (see also Fig. 4). Therefore, the northern and eastern parts of the modified AN01 geophysical/geotechnical model (Fig. 3) were extrapolated towards these directions. Due to the lack of detailed information on the 3-D geometry and material parameters of the formations in these areas, the modified AN01 model

Table 1. *P*-wave velocity α, *S*-wave velocity β, density ρ, *P*-wave quality factor Q_α and *S*-wave quality factor Q_β for the 3-D AN01 model (Anastasiadis *et al.* 2001).

Formation	$\alpha(\mathrm{m\,s^{-1}})$	$\beta(\mathrm{m\,s^{-1}})$	$\rho(\mathrm{g\,cm^{-3}})$	Q_α	Q_β
A	1050	250	2050	260	15
B	1850	180	2300	1130	25
C	1900	300	2150	510	20
E/F	3000	700	2350	690	50
Bedrock	4500	2000	2600	450	200
At free surface					
Bedrock (1000 m)	6000	3400	2600	450	200

was arbitrarily expanded by adopting the formation geometry of the model's Northern and Eastern edge and the dominant local Alpine trend of the sedimentary and bedrock formations in the area (NW–SE), also seen in the general geological outline and morphology presented in Figs 2a and 4. In other words, the Northern and Eastern model vertical cross-sections were replicated and appropriately shifted to obtain a bedrock-sediment surface geometry that matches the surface geology (bedrock-sediment contact) and geomorphology. The final computational model dimensions after this extrapolation are shown in Table 2 and its spatial extent is seen in Fig. 4. The framed areas correspond to the modified AN01 model.

It should be noted that this extrapolation approach, despite being only roughly realistic, is not expected to significantly affect the obtained results, since seismic waves generated at typical focal depths (5–10 km) and propagating towards Thessaloniki area (southwestern part of the model) are not generally influenced by, for example the presence of a small isolated surface sedimentary basin on top of the bedrock formation, just above the hypocentral area. Furthermore, the geometry of the artificially generated southeastern and northwestern sections of the enlarged model suggests that no waves travelling in these model parts will influence the main characteristics of the wave propagation in the broader Thessaloniki metropolitan area (southwestern part of the model of Fig. 4). This assumption was verified by both qualitative and quantitative tests (e.g. adopting different model enlargement strategies).

Given the size of the desired computational model and *S*-wave velocities in the model, the size of the spatial grid spacing was chosen to be 15 m in the finer grid. Assuming 6 grid spacings per minimum *S*-wavelength as sufficient spatial sampling, the maximum frequency up to which the simulation can be considered as sufficiently accurate is 2 Hz. Given the maximum *S*-wave velocity in the model, 3400 m s^{-1} and the smallest horizontal dimension of the model, 16 200 m, the simulation should only be considered for frequencies larger than 0.2 Hz. The time step for the FD computations was estimated using the equation:

$$\Delta t \leq \frac{6}{7\sqrt{3}} R, \quad R = \frac{\Delta h_{\min}}{V_{P\max}}, \tag{9}$$

where $\Delta h_{\min}$ is the minimum grid step used in the computation and $V_{P\max}$ is the maximum *P*-wave velocity of the computational model (Moczo *et al.* 2000). The time step estimated from eq. (9) for the simulations is 0.0012 s and the computational parameters are summarized in Table 2.

Six earthquake scenarios were considered, with two different focal mechanisms for each of three hypocentral positions examined. The computational model together with the epicentres and focal mechanisms of the earthquake scenarios are shown in Fig. 4. Geographical coordinates and focal parameters are summarized in Table 3. The same moment magnitude ($M_{5.1}$) and the hypocentral depth (5 km) was assumed for each of the six earthquakes. One additional numerical simulation was performed for a hypocentral depth of 10 km for the epicentral position 1.

A double-couple point source was assumed for each scenario. For the source–time function, representing particle velocity, a Gabor signal was assumed of the form,

$$s(t) = \exp\left\{-\left[\omega(t - t_s)/\gamma\right]^2\right\} \cos\left[\omega(t - t_s) + \theta\right], \tag{10}$$

where $\omega = 2\pi f_p$, $t \in [0, 2t_s]$, f_p is the dominant frequency, γ controls the width of the signal and θ is the phase shift. The source–time function parameters are given in Table 4, whereas the signal and its Fourier spectrum are shown in Fig. 5.
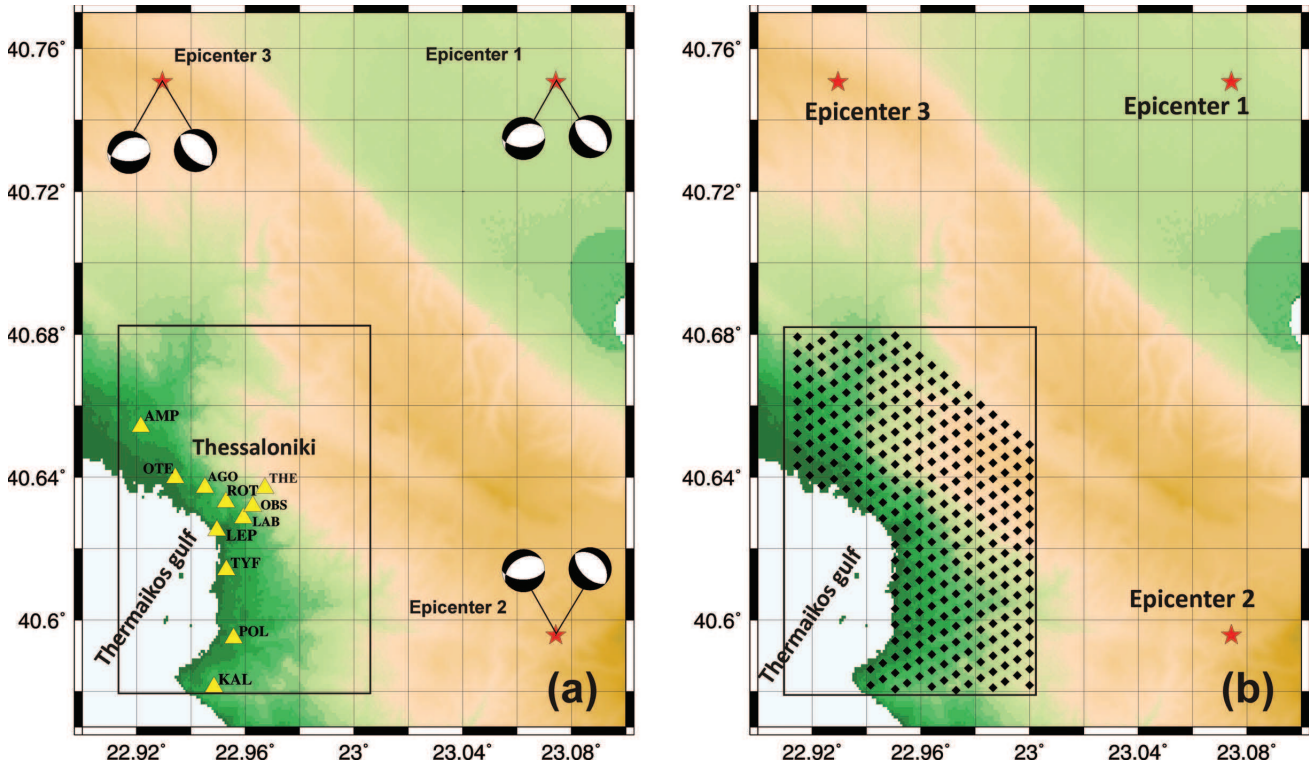
Figure 4. (a) Earthquake locations used for the seismic scenarios (red stars). The focal mechanisms used for each scenario are also shown. The sites where observed data and FD synthetics are available are shown with yellow triangles. (b) Grid of receivers used for studying the spatial variation of Fourier spectra for the six earthquake scenarios. The area covered corresponds to the area of the computational model, while the bounded area to the modified AN01 model (see text for details).

Table 2. Computational model parameters

Model dimensions: $X = 22\,545$ m, $Y = 16\,200$ m, $Z = 12\,105$ m
Grid spacing: 15 m in the finer grid $(0 - 1170$ m), 135 m in the coarser grid
Number of grid cells: $(1503 \times 1080 \times 78) + (167 \times 120 \times 81) = 128\,235\,960$
Frequency range: 0.2–2.0 Hz
Time step: 0.0012 s
Time window: 20 s
PML zone thickness: 90 grid spacings in the finer grid
10 grid spacings in the coarser grid

Table 3. Focal parameters of the earthquakes used for the computation of synthetic waveforms. All earthquakes have the same moment magnitude ($M_{5.1}$) and focal depth (5 km), except when otherwise specified in the text.

A/A	Lon. (E)	Lat. (N)	Strike	Dip	Rake
1a	23.0743	40.7506	90	55	−70
1b	23.0743	40.7506	135	55	−90
2a	23.0743	40.5977	90	55	−70
2b	23.0743	40.5977	135	55	−90
3a	22.9295	40.7506	90	55	−70
3b	22.9295	40.7506	135	55	−90

Table 4. Source time function parameters used in the FD computations.

	γ	f_p	θ	t_S
Scenarios 1, 2, 3	0.25	0.2	$\pi/2$	1.0

spatial variation of the simulated motion in the metropolitan area of Thessaloniki (Fig. 4, right-hand panel).

5 EVALUATION OF SITE RESPONSE

The accuracy of the model used in the computations is a critical issue that affects the accuracy and credibility of the resulted waveforms; therefore, it was necessary to further evaluate its impact on the determined site response. For this reason, two different approaches for the model extension procedure (described in the previous paragraph) have been implemented and the corresponding synthetic results have been produced. The first approach involves the extension of the model to the North, assuming a dominant N–S direction
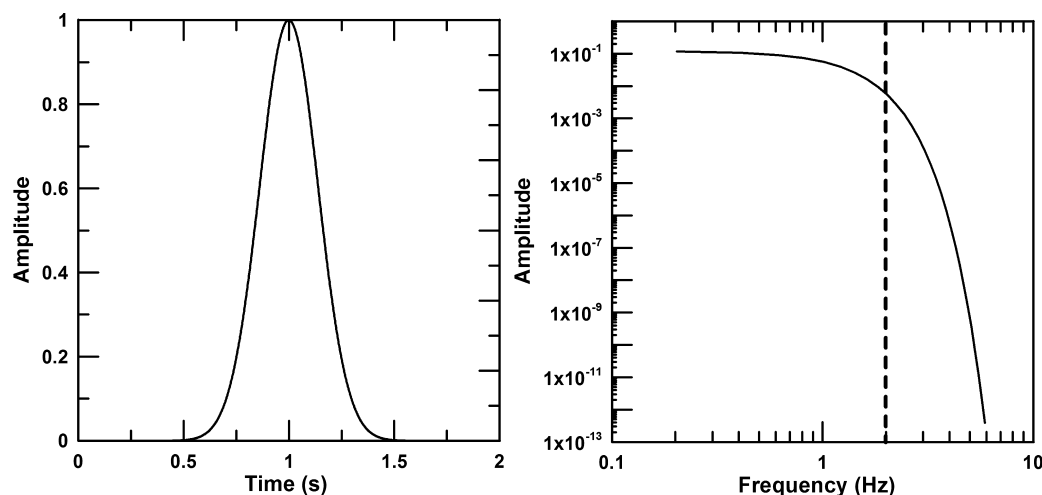
For the receivers 11 grid positions were chosen, corresponding to sites for which seismic records were available from a local network of seismographs and accelerographs that operated in the broader area of Thessaloniki during 4 months (November 1993–February 1994, Lachet *et al.* 1996). Fig. 4 (left-hand panel) shows the receiver positions and Table 5 lists code names and coordinates. Moreover, a dense grid of receiver positions was also considered to study the

Figure 5. (Left) Source time function used for FD computations. (Right) Fourier spectrum of the source time function used in the FD simulations. The vertical dashed line denotes the maximum theoretical frequency up to which FD computations can be considered sufficiently accurate (2 Hz).

Table 5. Code names and coordinates of examined sites, where experimental data were also available for comparison.

A/A	Code name	Lon. (E)	Lat. (N)
1	AGO	22.9459	40.6374
2	AMP	22.9215	40.6541
3	KAL	22.9485	40.5812
4	LAB	22.9592	40.6285
5	LEP	22.9495	40.6251
6	OBS	22.9628	40.6318
7	OTE	22.9343	40.6398
8	POL	22.9557	40.5949
9	ROT	22.9529	40.6330
10	THE	22.9670	40.6370
11	TYF	22.9530	40.6140

for the bedrock-sediments interface, that is practically replicating towards the North the northernmost E–W trending slice of the basic model of Fig. 2b. The second approach corresponds to the procedure described in the previous paragraph, which involves the same extension adopting the dominant NW–SE direction of the bedrock-sediments boundary, also shown in Fig. 2a. Comparisons for the two models expansion procedures were performed for two of the sites where empirical SSR were available, namely site AMP which is the closest to the NW part of the model which was expanded and site AGO located in the centre of the model. In Fig. 6 the results of this comparison both in the time and frequency domain for scenario 1a are presented, showing that the two different model expansion approaches have, practically, no impact on the synthetic waveforms. Moreover, the wave propagation characteristics that are presented in a video file compiled from the time snapshots of the N–S component for the model with the NW–SE extension of the bedrock (included in the Supporting Information) also verify the previous conclusions, as almost no backscattering from this expanded part of the model towards the main model body (including the 11 sites) is observed (Appendix S1).

The evaluation of site response was performed using the SSR approach (Borcherdt 1970). The geometric mean of smoothed FAS of the horizontal components for all six seismic scenarios was calculated and used for obtaining the synthetic SSR curves. Station OBS, which is located on bedrock, was used as a reference site, in

accordance with previous studies employing either real or synthetic recordings for the city of Thessaloniki. The synthetic SSR curves derived in this study have been compared with the empirical SSR curves from Lachet *et al.* (1996) (based on velocity recordings) and from Triantafyllidis *et al.* (2004b) (based on accelerograms).

All empirical and synthetic FAS were smoothed with the Konno & Ohmachi (1998) technique (smoothing parameter, $b = 20$), with the exception of original synthetic and empirical results from Triantafyllidis *et al.* (2004b), where a moving window of 0.5 Hz with a 50 per cent overlap was applied by the authors. In Fig. 7 comparisons between synthetic and empirical SSR curves are shown. The thick black curve corresponds to the average SSR curve from all six scenarios, whereas its standard deviation is shown by the dashed line. Empirical SSR curves by Lachet *et al.* (1996) (light blue) and Triantafyllidis *et al.* (2004a) (green) are also presented. The maximum frequency (f_{max}) up to which FD calculations in this study should be sufficiently accurate is denoted with a red line.

Comparisons between the empirical (Lachet *et al.* 1996; Triantafyllidis *et al.* 2004a) and the average synthetic SSR curves computed in this study (Fig. 7) are in a good agreement for the majority of the studied sites—both in terms of amplitudes and fundamental frequencies. Larger differences between the predicted and empirical SSR can be seen at sites where the model has been extended (e.g. sites AMP, KAL, see Fig. 2b). However, given the geophysical/geotechnical model inherent uncertainties, the numerical predictions can be characterized as satisfactory. Furthermore, it should be pointed out that the presented empirical SSR curves have been calculated from recordings of earthquakes at various epicentral distances, different magnitudes and focal mechanisms. On the other hand the SSR curves computed in this study from the FD simulations have been computed based on a limited number of earthquake scenarios and focal mechanisms, magnitudes and epicentral distances.

Results have been also compared with theoretical SSR curves from 1-D methods such as modal summation (Panza 1985; Panza & Suhadolc 1987) and reflectivity method (Kennett 1983), as applied by Triantafyllidis *et al.* (2004a) and Raptakis *et al.* (2004a), respectively. Comparisons with 2-D theoretical modelling were performed using results from the hybrid (Fah 1992) and FD method (Moczo 1989; Moczo & Bard 1993), as applied by Triantafyllidis *et al.* (2004a) and Raptakis *et al.* (2004b), respectively, for the broader
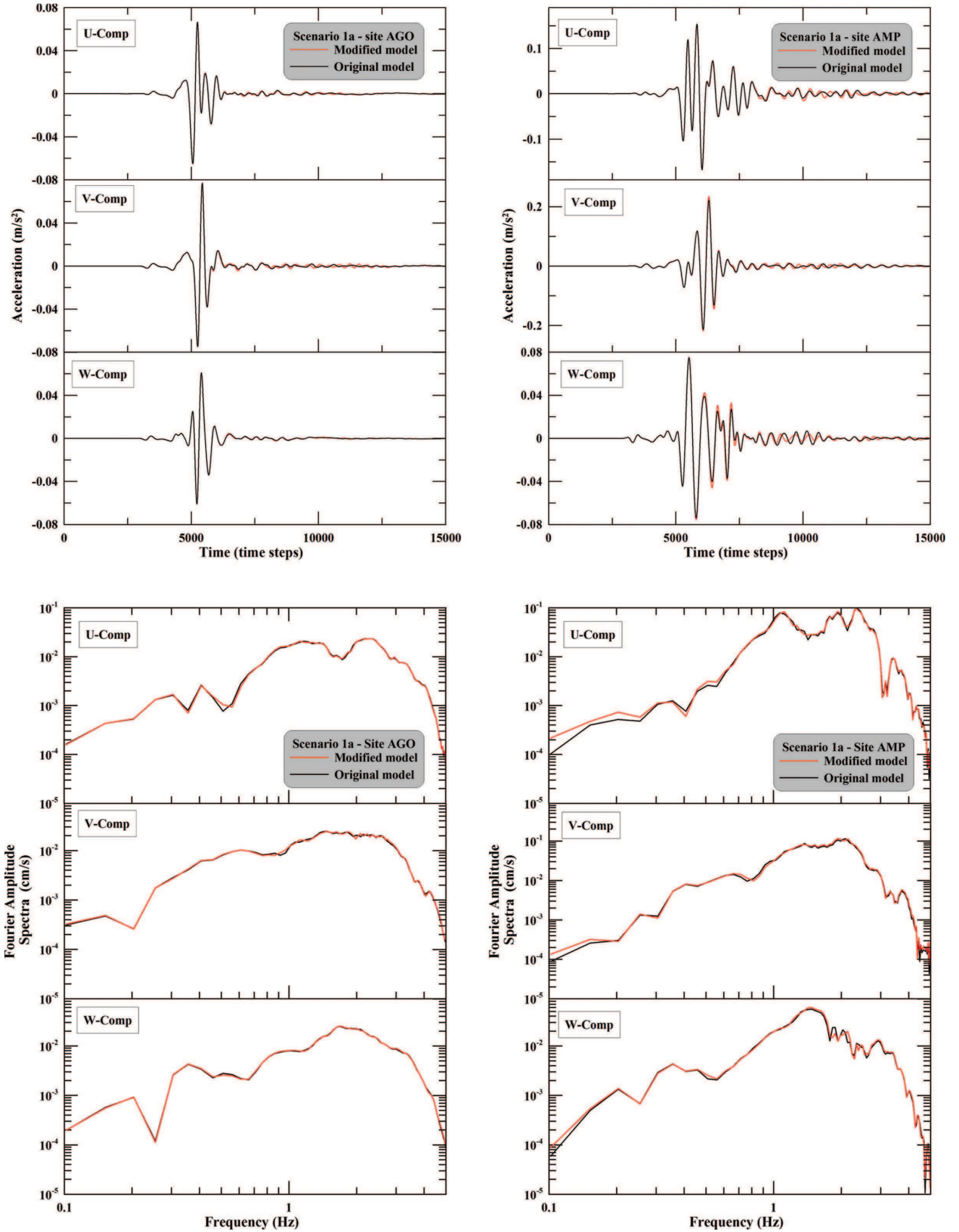
Figure 6. (Top) Comparisons of 3-D synthetics estimated from two different geophysical-geotechnical models for sites AGO and AMP and scenario 1a. (Bottom) Comparisons of FAS for sites AGO and AMP.
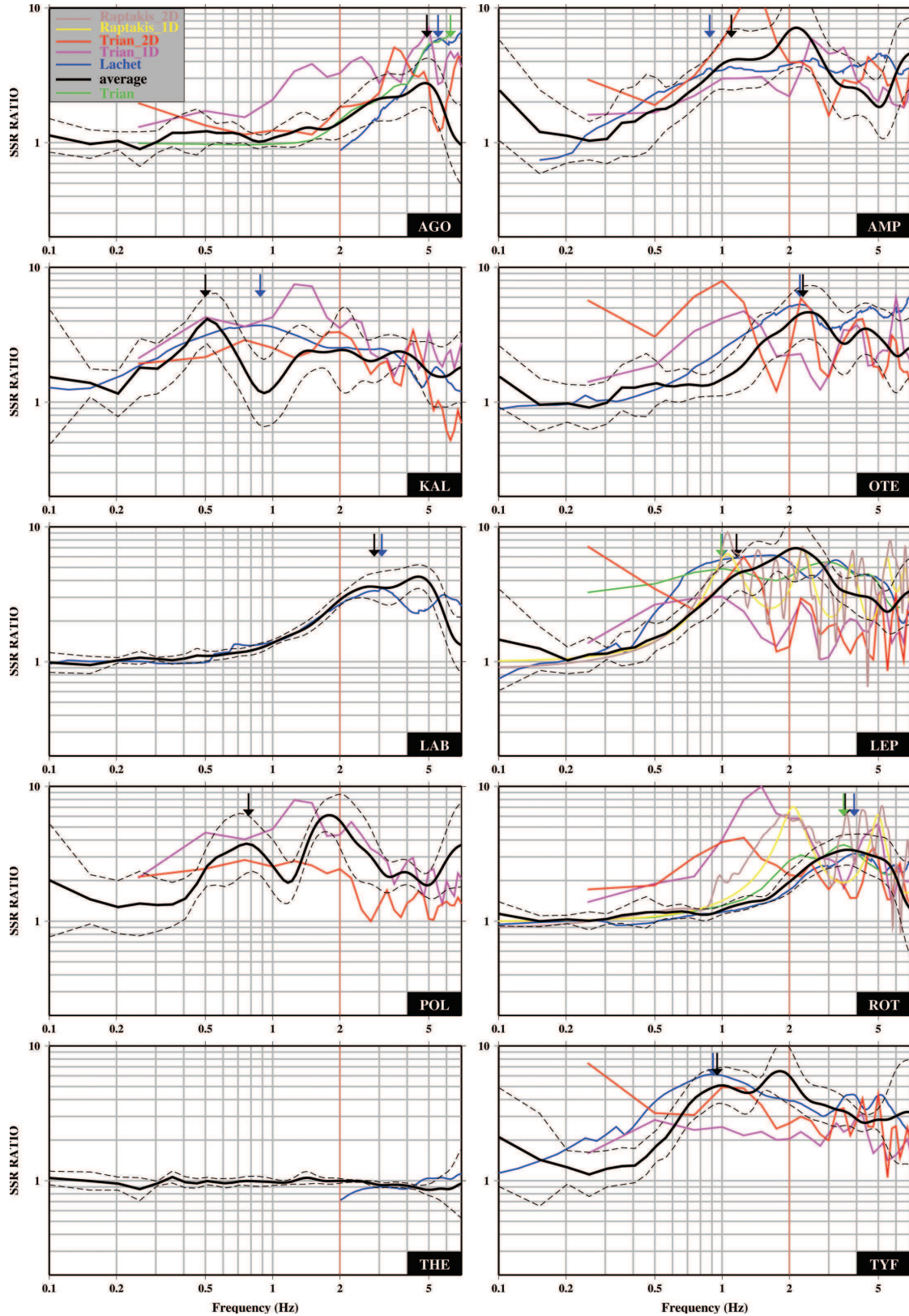
Figure 7. Average synthetic SSR curves from all six seismic scenarios (thick black line) and corresponding standard deviation (thin dashed black line) for the 10 examined sites. Empirical SSR curves derived by Lachet *et al.* (1996) and Triantafyllidis *et al.* (2004a) are denoted by the blue and green lines, respectively. Synthetic curves from 1- and 2-D numerical modelling by Triantafyllidis *et al.* (2004b) (pink and red) and by Raptakis *et al.* (2004b) (yellow and brown) are also shown. The red vertical line shows the maximum frequency (f_{max}) up to which FD calculations in the present study can be considered sufficiently accurate. Colored arrows denote the fundamental frequencies of the corresponding SSR curves.

area of Thessaloniki. The theoretical SSR curves from the 1-D and 2-D numerical modelling are also shown in Fig. 7.

The results presented in Fig. 7 clearly demonstrate that the average 3-D model synthetic SSR curves estimated in this study exhibit a superior performance with respect to the 1-D and 2-D numerical modelling, regarding both the fundamental frequency and amplification levels derived from the observed SSR curves. It could be argued that the observed discrepancies, which are occasionally large (e.g. sites OTE, ROT) can be justified, to a certain extent, by the fact that 1-D and 2-D synthetics computed by the various researchers, were not based exactly on the same geophysical-geotechnical model. Therefore, even minor differences in the input model configuration used in the various studies may become important, especially for sites that are situated in the extrapolated areas of the AN01 model.

To examine this issue, additional synthetics (1-D synthetics hereinafter) have been computed with the program Axitra [program by O. Coutant based on Discrete Wavenumber Method (DWN) by Bouchon 1981] for each site using the local 1-D structure extracted from the constructed 3-D model. For the simulation a point-source (3-D wavefield), with the same properties as the one used in FD simulations, has been used to account only for the 1-D structure effects in the SSR comparisons. Therefore the term "1-D synthetics" actually refers to synthetics for 1-D structure and not to synthetics for 1-D structure and 1-D wavefield. Comparisons between average 3-D (black solid) and 1-D (black dashed) synthetic SSR curves are shown for the six scenarios in Fig. 8a, where the observed SSR curves (grey curves) by Lachet *et al.* (1996) are also superimposed. In these figures, similar behaviour as the one described in Fig. 7 can be identified for the majority of the studied sites, with the 3-D SSR curves exhibiting a much better agreement with the observed SSR results, regarding both the fundamental frequency and SSR amplitude and shape characteristics.

This agreement is further quantified in Fig. 8b, where the empirical fundamental frequency and the corresponding SSR amplification from Lachet *et al.* (1996) is plotted against the theoretical results from both 1-D and 3-D simulations. In almost all cases the results from the 3-D modelling are much better correlated with the observed (empirical) SSR frequencies and amplitudes. Given that the local geophysical model employed and source properties are the same, the differences between 1-D and 3-D results reflect the lower efficiency of the 1-D simulations in describing the site response for the examined sites. An exception is the amplification amplitude for station AGO, which is the site with the highest fundamental frequency (small sedimentary cover thickness). This discrepancy is probably due to the fact that the employed FD modelling should be sufficiently accurate up to 2 Hz and practically of acceptable accuracy up to $\sim$4–4.5 Hz, as is evident from the variability of the individual SSR results from the different scenarios later presented (Figs 9 and 10). Therefore, the frequency and especially the theoretical SSR amplitudes for station AGO (fundamental frequency from 3-D model $\sim$5 Hz) should be considered as inaccurate.

As was pointed out by other researchers (e.g. Makra *et al.* 2002; Semblat *et al.* 2005) who compared results from 1-D and 2-D analysis, higher-order simulations tend to predict higher amplifications, which are also shifted towards higher resonant frequencies when compared to those predicted from lower-order simulations. This effect is attributed to the contribution of the models' lateral heterogeneities in the amplification of ground motions. In other words, the effect of lateral heterogeneity of the model on propagation of surface waves, results in more pronounced amplification shifted towards higher frequencies.

The previously described pattern is also observed in the 3-D synthetics calculated in this study (see Fig. 8a and left-hand panel of Fig. 8b). This is more evident in Fig. 9a, where the relative increase of the fundamental frequency estimated from FD simulations (F3D) with respect to the one from the DWN simulations (F1D) is plotted against F1D. A clear, almost linear, increase of the relative frequency shift with respect to F1D can be observed for sites with F1D spanning the range 0.5–2.5 Hz (F3D 0.5–3.5 Hz), with the exception of site AGO, for which the relative change can be considered as inaccurate, as previously explained. The three sites (OTE, LAB and ROT) exhibiting the higher relative values of frequency shifting are located on intermediate thickness soil formations (F1D $\sim$1.5–2.5 Hz), verifying the correlation of the frequency shifting with the local site's structure (higher frequency shifting for higher F1D).

In Fig. 9b the relative increase of the 3-D SSR fundamental amplitude (AMP3D), with respect to the one of 1-D simulations (AMP1D), is plotted against AMP1D. The most prominent feature is the high relative values of 3-D to 1-D amplifications observed in the coastal zone, as defined by sites TYF, LEP and possibly POL (see also Fig. 4). This zone is characterized by relatively thick soil formations and high absolute values of amplifications. Most of the other sites studied do not exhibit noteable relative SSR amplification changes (maximum variation of $\sim$±20 per cent).

It should be pointed out that for some sites (e.g. LEP and TYF), located in the area of the Thessaloniki's city centre, a good agreement, is found between results from 2-D and 3-D numerical modelling. This agreement only concerns the predicted fundamental frequency for the examined sites and not the amplitude or the general shape characteristics of the corresponding SSR curves. This observation supports the findings of other researchers (e.g. Panou *et al.* 2005) who showed the dominant control of the 2-D geometry of soil formations on the site response characteristics. Nevertheless, the majority of comparisons between results from 1-D, 2-D and 3-D numerical modelling confirm the significant impact of the 3-D model structure on the detailed characteristics of seismic motion for the broader Thessaloniki area.

6 DEPENDENCE OF SITE RESPONSE ON SOURCE AND MODEL GEOMETRY

The variability of the mean SSR depicted by the corresponding standard deviation (Fig. 7—black dashed lines) is a consequence of the differences between the individual SSR ratios of the six scenarios studied. These differences are found not only among scenarios with different hypocenter locations, but also between scenarios with the same hypocenter location and different focal mechanisms. The influence of the focal mechanism on the local amplification of the seismic motion has been identified also by other researchers (e.g. Field 1996; Riepl *et al.* 1998) as a factor that could significantly bias the estimated site response. An example is given in Fig. 10, where for four selected sites the SSR curves from six scenarios are shown (red, green and blue dashed and solid lines), together with the mean curve (black line) and empirical SSR curves (light blue) from Lachet *et al.* (1996). In some cases, for example for site TYF, strong differences are observed between scenarios 2 (blue solid and dashed curves, which correspond to different focal mechanisms) both in terms of amplitude and fundamental frequency, in the frequency range 0.2–4 Hz. For site POL these differences are found in both scenarios 1 (red curves) and 2 (blue curves) for the same frequency window. On the other hand, there are sites, for example
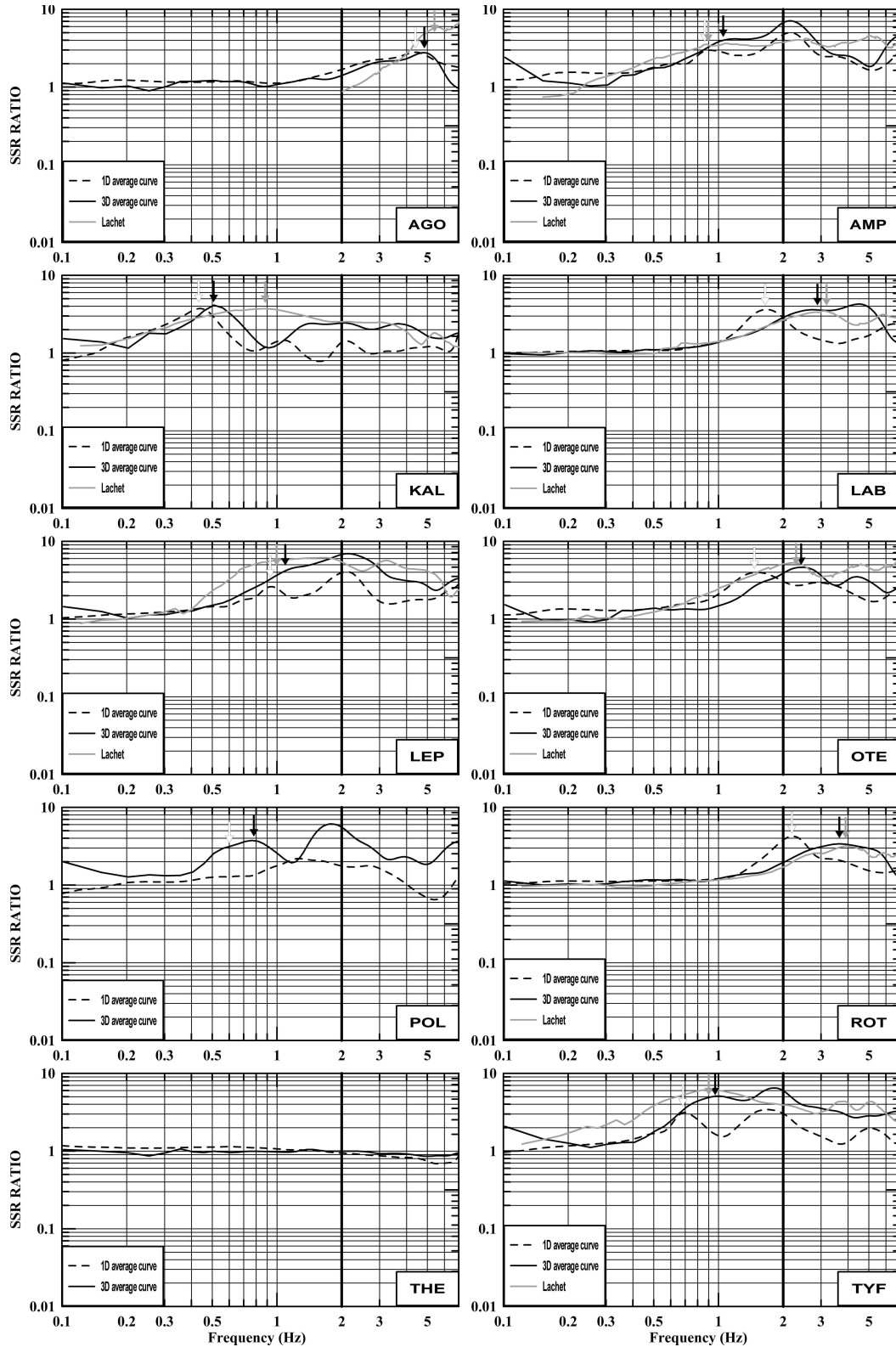
Figure 8. (a) Average synthetic SSR curves from 3-D (FD synthetics-solid line) and 1-D (DWN synthetics-dashed line) numerical modelling for the six scenarios. The observed SSR curves from Lachet *et al.* (1996) are also plotted for comparison (grey line). The black vertical line corresponds to the maximum frequency (f_{max}) up to which FD calculations of the present study can be considered sufficiently accurate. Black, white and grey arrows denote the fundamental frequencies of the corresponding SSR curves. (b) Comparison between the 3-D (circles) and 1-D (squares) model and the empirical fundamental frequencies (left) and amplification amplitudes (right), as derived from the corresponding SSR curves. The superiority of the 3-D results is evident in both cases. Station AGO, for which the 3-D FD results should be considered as inaccurate, is denoted by a grey solid circle.
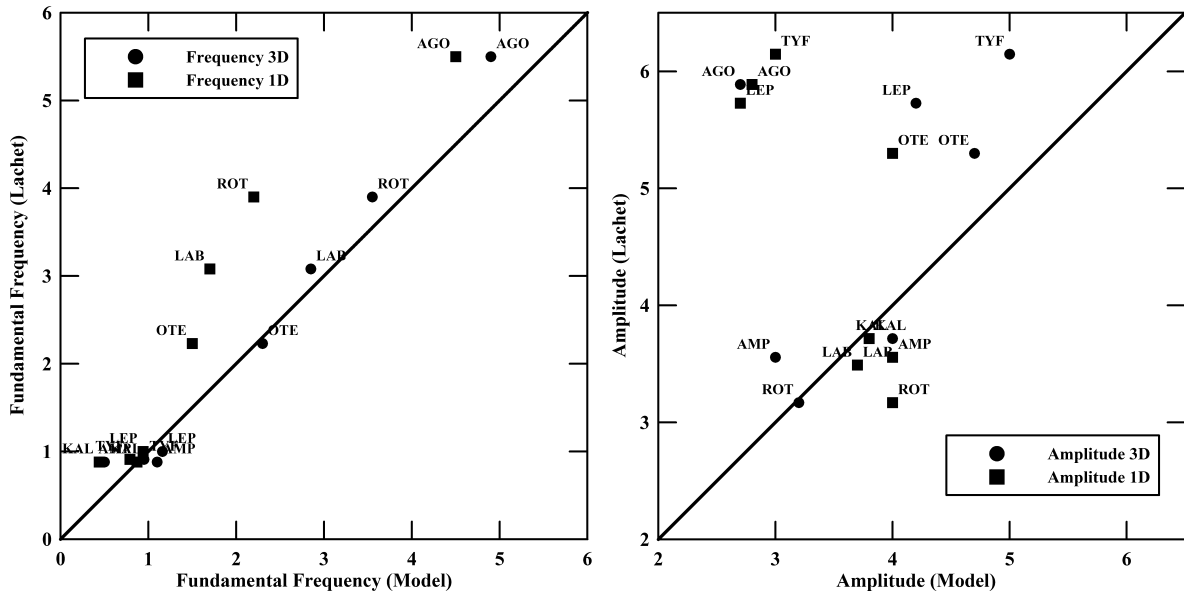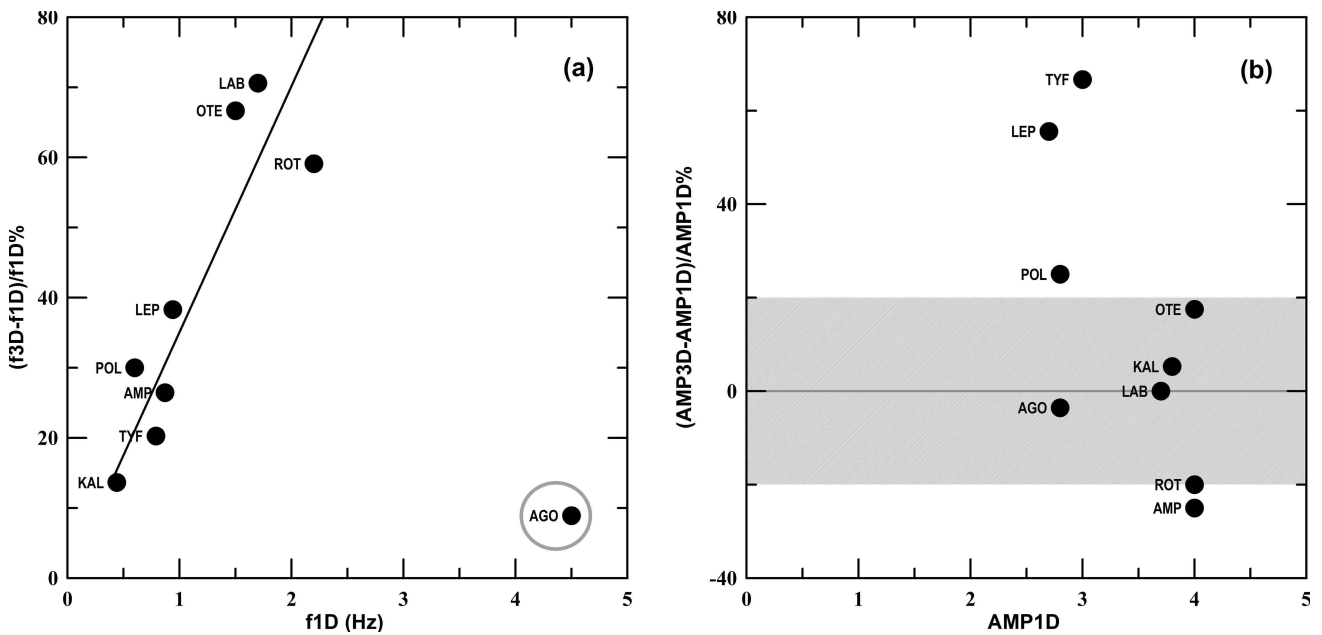
Figure 8. (*Continued.*)

Figure 9. (a) Relative variation of 3-D model fundamental frequency with respect to the corresponding 1-D one, plotted against the 1-D fundamental frequency for each site. (b) Relative variation of 3-D SSR fundamental amplitudes plotted against the 1-D SSR amplitude for each site. Station AGO, for which the 3-D FD results should be considered as inaccurate, is denoted by a grey solid circle.

LAB and ROT, where all six scenarios produce quite similar results, with little variability.

Similar conclusions are drawn when the dependence of local site response on the focal depth of the earthquake is examined. For this reason scenarios 1a and 1b have been computed using a focal depth of 10 km and compared with the ones computed for a depth of 5 km. Comparisons are shown in Fig. 11, where the SSR curves for 5 and 10 km are denoted with the red and green colours, respectively. Average SSR curve (black) from six scenarios and empirical SSR curves by Lachet *et al.* (1996) (light blue) are also shown. For the

majority of examined sites, comparisons show that local site effects also depend on the focal depth of the earthquake, but not as significantly as on the focal mechanism. Again, there are sites that exhibit practically the same SSR pattern, independently of the focal depth of the earthquake (e.g AGO, LAB, ROT), whereas sites with thicker soil formations (e.g. KAL, LEP, TYF) show differences, mostly in the predicted amplification levels (in most cases lower amplifications for the larger focal depth scenarios—green curves). The previous results imply that a unified and unique local site response cannot be determined for different seismic excitations, at least not
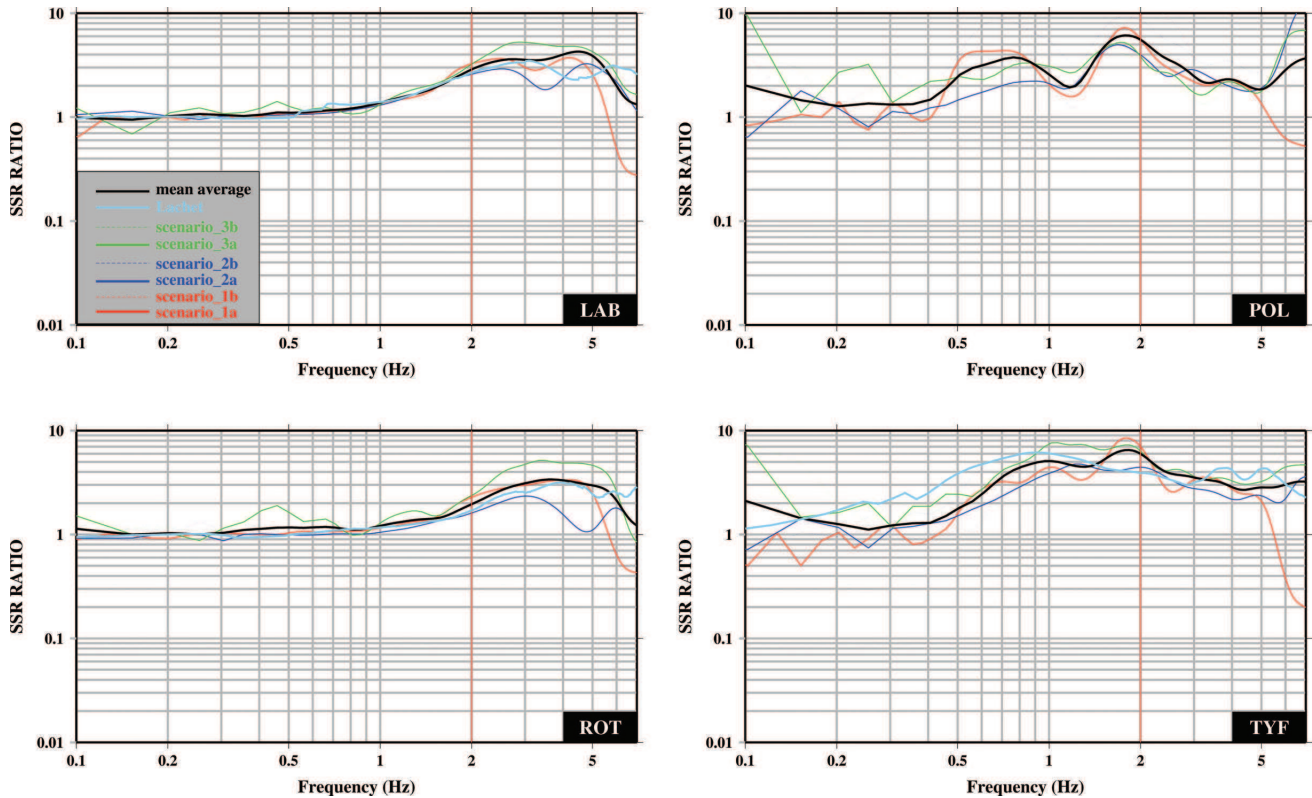
Figure 10. Synthetic SSR curves from 3-D numerical modelling for the six scenarios studied (see Table 2 for each scenario parameters). Average synthetic SSR curve (black) from six scenarios and empirical SSR curves by Lachet *et al.* (1996) (light blue) are also shown. The red vertical line shows the maximum frequency (f_{max}) up to which FD calculations in the present study can be considered sufficiently accurate.

for all sites studied, since a strong dependence of local site response on the source properties (focal mechanism, depth) and location is observed.

Nevertheless, except for the effect of the focal parameters, the geophysical model's structure itself remains the dominant factor controlling the local site response. To demonstrate the impact of the AN01 model on seismic motion for the broader area of Thessaloniki, the FAS spatial distribution was examined. FAS of ground acceleration have been computed for the dense grid of receivers (Fig. 4b), for all six scenarios. To minimize source (radiation pattern) and geometric spreading effects and enhance the effect of the 3-D geometry of soil formations, FAS were calculated for the AN01 geophysical model (FAS3D) and for the corresponding bedrock 1-D model (FAS1D). Therefore the (FAS3D)/(FAS1D) ratio mainly reflects the spectral amplification due to the 3-D structure of the geophysical model, with source and path effects partly eliminated.

In Fig. 12 the spatial variation of the examined ratios for the three components of ground motion is shown for the six scenarios studied and for the frequency of 1 Hz. The area covered in Fig. 12 corresponds to the area of the computational model. The N–S component exhibits the lowest spectral relative amplification values (FAS3D/FAS1D) for all six scenarios. For scenario 2a, though, for the north-western parts of the model the peak values predicted are much higher (∼9). For the E–W component the highest values are predicted for scenarios 1a and 3a for the south-eastern part of the model. Maximum amplification levels predicted are as high as 14–16 for scenario 1a and ∼10 for scenario 3a. For the remaining cases relatively high values of amplification (5–6) are found only

for smaller parts of the model, mostly in the centre of the metropolitan area of Thessaloniki. Vertical components exhibit, as expected, much lower amplification amplitudes than the horizontal ones. Nevertheless, the largest vertical amplification amplitudes are observed for scenarios (1) (up to ∼9), mostly in the central part of the coastal zone, where thicker sediments dominate the local structure. It has to be stressed that FAS spatial distribution has been studied for a larger set of periods, not shown here for practical reasons and a similar spatial distribution pattern as the one described in Fig. 12 has been observed.

7 DISCUSSION-CONCLUSIONS

In this study the site response for selected sites in the metropolitan area of Thessaloniki (Northern Greece) has been evaluated using the 3-D finite-difference modelling. Synthetic waveforms for six seismic scenarios with different source properties (hypocenter and focal mechanism) derived from the well-known seismotectonic characteristic of the broader area of Thessaloniki have been computed.

The geophysical-geotechnical 3-D model proposed in this study is based on both available 3-D models for the broader area of Thessaloniki, namely the results of Anastasiadis *et al.* (2001) (model AN01) and Apostolidis *et al.* (2004a, b) (model AP04). These two models do not cover the same area, with the AN01 covering mostly the broader area of the historical center of the city. The computational model used in the FD simulations is based mostly on the extended AN01 model (dynamic properties and layer geometry), as expanded to cover the whole area of interest, using either the
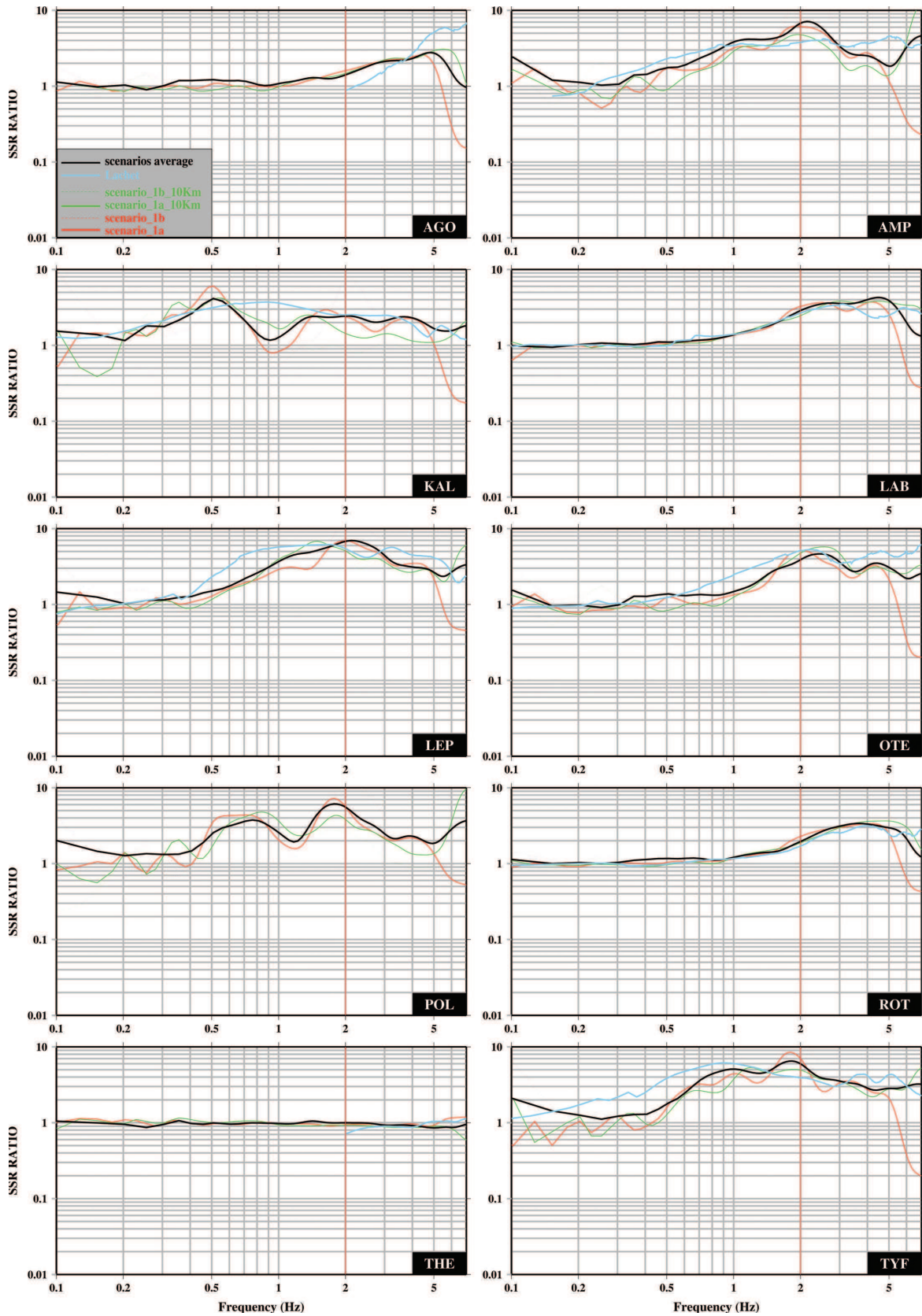
Figure 11. Synthetic SSR curves from 3-D numerical modelling for scenario 1 and focal depths of 5 km (red) and 10 km (green). Average SSR curves (black) from the six scenarios and empirical SSR curves by Lachet *et al.* (1996) (light blue) are also plotted. The red vertical line shows the maximum frequency (f_{max}) up to which FD calculations in the present study can be considered sufficiently accurate.
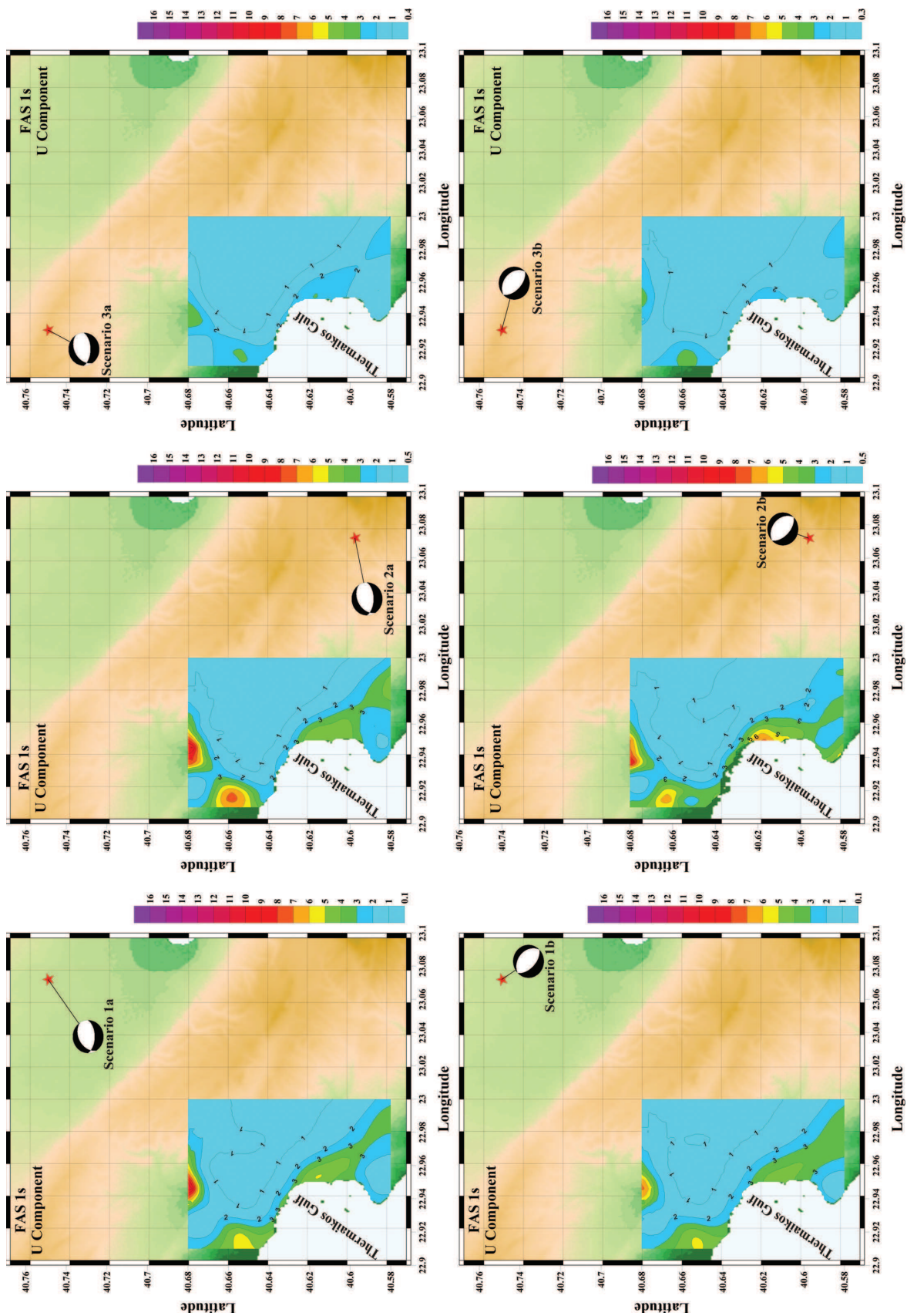
Figure 12. (a) Spatial variation of the average (FAS3-D)/(FAS1-D) ratio for the U component (N–S) for the six examined scenarios and frequency of 1 Hz for the final model area and receiver configuration (Fig. 4b). (b) Spatial variation of the average (FAS3-D)/(FAS1-D) ratio for the V component (E–W) for the six examined scenarios and frequency of 1 Hz for the final model area and receiver configuration (Fig. 4b). (c) Spatial variation of the average (FAS3-D)/(FAS1-D) ratio for the W component (vertical) for the six examined scenarios and frequency of 1 Hz for the final model area and receiver configuration (Fig. 4b).
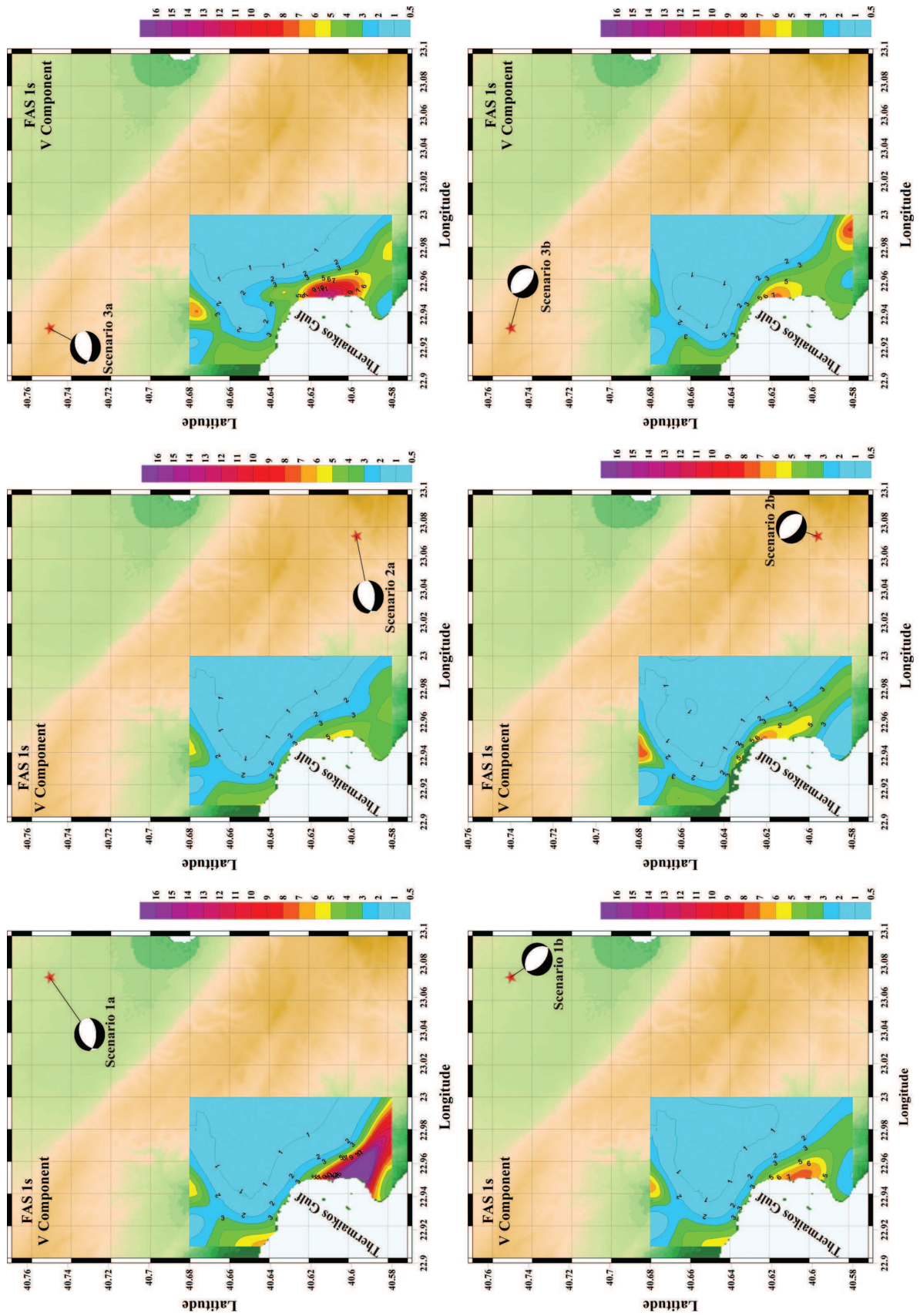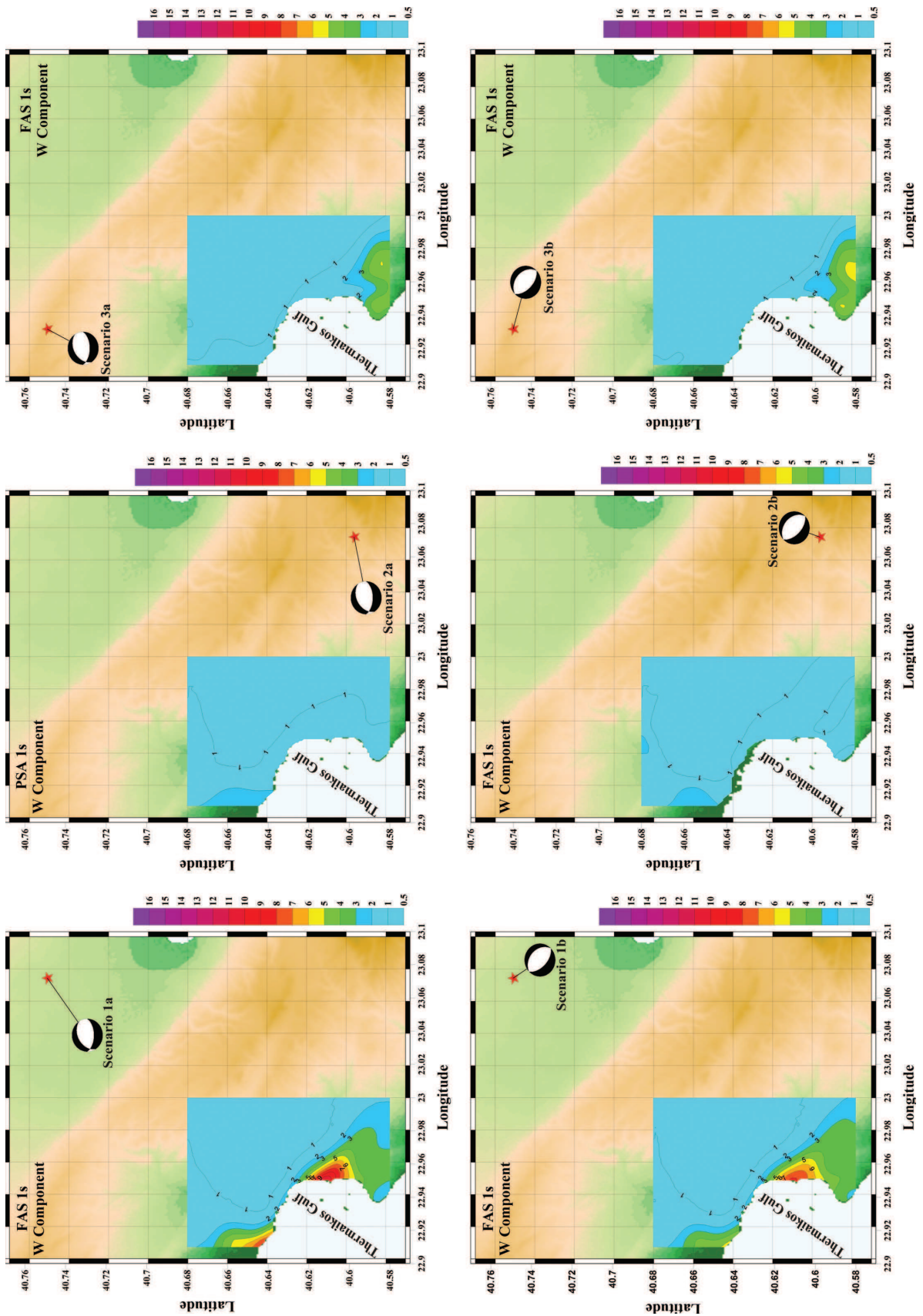
Figure 12. (*Continued.*)

Figure 12. (*Continued.*)

AP04 model or assumptions based on surface geology, which are not expected to significantly affect the simulations.

Comparisons have been performed between synthetic and empirical SSR spectral amplification curves. The average synthetic SSR curves from the six scenarios of the 3-D FD modelling are in a very good agreement with the empirical ones for the majority of the studied sites. These comparisons constitute strong evidence about the reliability of the obtained results, since empirical curves represent earthquakes with a much larger spatial variation in comparison to the FD synthetics that were computed for a relatively limited number of seismic scenarios.

Comparisons of the average synthetic 3-D SSR curves with SSR curves from 1-D and 2-D numerical modelling showed that in most of the cases the 3-D modelling and its corresponding SSR curves describe much more efficiently the spectral characteristics (in terms of fundamental frequency and site amplification) of the sites studied. Furthermore, the obtained results verify that 3-D simulations tend to predict higher amplifications mostly for the thicker sediments of the coastal zone, where high absolute values of SSR amplifications are found. Moreover, an almost linear relative fundamental frequency shift to higher values than those predicted from 1-D simulations is observed for thinner sedimentary cover sites (higher 1-D fundamental frequencies), with some sites (OTE, LAB and ROT) showing a >50 per cent or larger relative frequency shift. These results are in good agreement (but are also more pronounced) with earlier comparisons between 2-D and 1-D synthetics.

The relatively large standard deviation of the mean SSR for most examined sites is a direct consequence of the variability among the individual SSR of the six scenarios studied. In addition, similar behaviour is shown when the dependence of local site response on the focal depth of the earthquake is examined. These results imply that a single local site response cannot be uniquely determined for different seismic excitations, at least not for all studied sites of the city of Thessaloniki, since a strong dependence of local site response on both focal mechanism and hypocenter location has been observed.

It should be noted, however, that the 3-D geophysical-geotechnical model structure still plays a dominant role in forming the local site response. The impact of the employed AN01 model on seismic motion for the broader area of Thessaloniki is more clearly examined by using the spatial variations of the relative FAS amplifications. The results of the FAS study, together with the aforementioned ones, verify that the variations among scenarios with different hypocenters (scenarios 1, 2 and 3) and different focal mechanisms (scenarios a and b), are a consequence of the dependence of local site response on various parameters (source parameters, location and model structure), for different seismic excitations. This result suggests that, generic or even 1-D local site responses should be used with caution when studying soil and structure behaviour for specific earthquakes, at least for the Thessaloniki area.

In most of the cases the previous results exhibit the superiority of 3-D-FD simulations in comparison with the 1-D and 2-D ones, in predicting SSR fundamental frequencies and amplification levels for several sites in the area of Thessaloniki. However, in future studies, assuming that the quality and the number of the available empirical data would be sufficiently adequate, the non-linear behaviour of soil formations should be also taken into account in simulations for the realistic estimation of 3-D-SSR, in cases of strong seismic excitation.

REFERENCES

Anastasiadis A., Raptakis, D. & Pitilakis, K., 2001. Thessaloniki's detailed microzoning: subsurface structure as basis for site response analysis. *Pure appl. Geophys.,* **158,** 2597–2633.

Apostolidis P., Raptakis, D. & Pitilakis, K., 2004a. The use of microtremors for the definition of soil properties and bedrock depth in an urban area, in *Proceedings of the 13th World Conference On Earthquake Engineering,* Vancouver, BC, Canada.

Apostolidis P., Raptakis, D., Roumelioti, Z. & Pitilakis, K., 2004b. Determination of *S*-wave velocity structure using microtremors and SPAC method applied in Thessaloniki (Greece), *Soil Dyn. Earthq. Eng.,* **24,** 49–67.

Borcherdt, R.D., 1970. Effects of local geology on ground motion near San Francisco Bay, *Bull. seism. Soc. Am.,* **60,** 29–61.

Bouchon, M., 1981. A simple method to calculate Green's functions for elastic layered media, *Bull. seism. Soc. Am.,* **71,** 959–971.

Chávez-García F.J., Pedotti, G., Hatzfeld, D. & Pierre-Yves B., 1990. An experimental study of site effects near Thessaloniki (northern Greece), *Bull. seism. Soc. Am.,* **80,** 784–806.

Fäh, D., 1992. A hybrid technique for the estimation of strong ground motion in sedimentary basins, *Ph.D. Thesis.* Nr 9767, Swiss Federal Institute of Technology, Zurich.

Field, E.H., 1996. Spectral amplification in a sediment-filled valley exhibiting clear basin-edge induced waves, *Bull. seism. Soc. Am.,* **86,** 991–1005.

Kennett, B.L.N., 1983. *Seismic Wave Propagation in Stratified Media,* Cambridge University Press, Cambridge.

Kobayashi H., 1974. Preliminary Report on the Microtremor Measurements in Thessaloniki, UNPD/SFREM.70.172.

Konno, K. & Ohmachi T., 1998. Ground-motion characteristics estimated from spectral ratio between horizontal and vertical components of microtremor, *Bull. seism. Soc. Am.,* **88,** 228–241.

Kristek, J., Moczo, P. & Archuleta, R.J., 2002. Efficient methods to simulate planar free surface in the 3D 4th-order staggered-grid finite-difference schemes, *Studia geophys. Geod.,* **46,** 355–381.

Kristek, J. & Moczo, P., 2003. Seismic wave propagation in viscoelastic media with material discontinuities—a 3D 4th-order staggered-grid finite-difference modeling, *Bull. seism. Soc. Am.,* **93,** 2273–2280.

Kristek, J., Moczo, P. & Galis, M., 2009a. A brief summary of some PML formulations and discretizations for the velocity-stress equation of Seismic motion. *Studia Geophys. Geod.,* **53,** 459–474.

Kristek, J., Moczo, P. & Pazak, P., 2009b. Numerical modeling of earthquake motion in Grenoble basin, France, using a 4th-order velocity-stress arbitrary discontinuous staggered-grid FD scheme, in *ESG 2006, Third International Symposium on the Effects of Surface Geology on Seismic Motion,* Vol. 2, paper S12, pp. 10, eds Bard, P.-Y., Chaljub, E., Cornou, C., Cotton, F. & Gueguen P., LCPC Editions, Grenoble, ISBN 978-2-7208-2494-1.

Lachet C., Hatzfeld, D., Bard, P.-Y., Theodulidis, N., Papaioannou, Ch. & Savvaidis, A., 1996. Site effects and microzonation in the city of Thessaloniki (Greece) comparison of different approaches, *Bull. seism. Soc. Am.,* **86,** 1692–1703.

Lalechos, N. & Savoyat, E., 1979. La sedimentation Neogene dans le Fosse Nord Egeen, in *Proceedings of the 6th Colloqium on the Aegean Region,* Athens, Greece, **2,** pp. 591–603.

Leventakis G. & Roussopoulos, A., 1974. Progress Report on Microzoning in Greece by the Greek Working Group, Athens.

Makra K., Raptakis, D., Chavez-Garcia, F.J & Pitilakis, K., 2002. How important is the detailed knowledge of a 2D soil structure for site response evaluation? In *Proceedings of the 12th European Conference on Earthquake Engineering,* 9–13 September, London, UK.

Moczo, P., 1989. Finite-difference technique for SH-waves in 2-D media using irregular grids—application to the seismic response problem, *Geophys. J. Int., 99,* 321–329.

Moczo, P. & Bard, P.-Y., 1993. Wave diffraction, amplification and differential motion near strong lateral discontinuities, *Bull. seism. Soc. Am., 83,* 85–106.

Moczo, P., Kristek, J. & Halada, L., 2000. 3D 4th-order staggered-grid finite difference schemes: stability and grid dispersion, *Bull. seism. Soc. Am., 90,* 587–603.

Moczo, P., Kristek, J., Vavryčuk, V., Archuleta, R.J & Halada, L., 2002. 3D heterogeneous staggered-grid finite-difference modeling of seismic motion with volume harmonic and arithmetic averaging of elastic moduli and densities, *Bull. seism. Soc. Am., 92,* 3042–3066.

Moczo, P., Kristek, J., Galis, M., Pazak, P. & Balazovjech, M., 2007. The finite-difference and finite-element modeling of seismic wave propagation and earthquake motion, *Acta Physica Slovaca, 57,* 177–406.

Panou A.A., Theodulidis N., Hatzidimitriou P., Stylianidis K. & Papazachos C.B., 2005. Ambient noise horizontal-to-vertical spectral ratio in estimating site effects and seismic damage distribution in urban environment: the case of Thessaloniki city (Northern Greece), *Soil Dyn. Earthq. Eng., 25,* 261–274.

Panza, G.F., 1985. Synthetic seismograms: the Rayleigh waves modal summation, *J. Geophys., 58,* 125–145.

Panza, G.F. & Suhadolc, P., 1987. Complete Strong Motion Synthetics, in *Seismic Strong Motion Synthetics, Computational Techniques,* Vol. 4, pp. 153–204, ed. Bolt, B.A., Orlando, Academic Press.

Papazachos B.C. & Papazachou, A., 2002. *Earthquakes of Greece,* Ziti Publications, Thessaloniki, 304 pp.

Papazachos, B.C., Tsapanos, T.M. & Panagiotopoulos, D., 1983. The time, magnitude and space distribution of the 1978 Thessaloniki seismic sequence, in *The Thessaloniki northern Greece earthquake of June 20, 1978 and its seismic sequence. Technical chamber of Greece, section of central Macedonia,* pp. 117–131.

Pitilakis K., Tsotsos, S. & Hatzigogos, Th., 1982. Study of liquefaction potential in the area of Thessaloniki, in *Proceedings of the 7th Symposium on Earthquake Engineering,* Sarita Prakashan, Meerut, India.

Raptakis D., Anastasiadis, A. & Pitilakis, K., 1998. Preliminary instrumental and theoretical approach of site effects in Thessaloniki, in *Proceedings of the 11th European Conference on Earthquake Engineering,* Rotterdam, Netherlands.

Raptakis D., Makra, K., Anastasiadis, A. & Pitilakis, K., 2004a. Complex site effects in Thessaloniki (Greece). Part I. Soil structure and comparison of observations with 1D analysis, *Bull. Earth. Eng., 2,* 271–300.

Raptakis D., Makra, K., Anastasiadis, A. & Pitilakis, K., 2004b. Complex site effects in Thessaloniki (Greece). Part II. 2D SH modeling and engineering insights, *Bull. Earth. Eng., 2,* 301–327.

Riepl J., Bard, P.-Y., Hatzfeld, D., Papaioannou, C. & Nechtschein, S., 1998. Detailed evaluation of site-response estimation methods across and along the sedimentary valley of Volvi (EURO-SEISTEST), *Bull. seism. Soc. Am., 88,* 488–502.

Roussos, N., 1994. Stratigraphy and paleogeographic evolution of the Paleocenemolassic basins of the North Aegean area, *Bull. Geol. Soc. Greece, 30,* 275–294.

Semblat J.F., Kham, M., Parara, E., Bard, P.Y, Pitilakis, K., Makra, K. & Raptakis, D., 2005. Seismic wave amplification: basin geometry vs soil layering, *Soil Dyn. Earth. Eng., 25,* 529–538.

Sherif M.A., 1973. Microzonation of Thessaloniki, using the Sherif-Bostrom (USA) method, *UNDP/UNESCO Survey of the Seismicity of the Balkan Region,* Seattle, Washington, USA.

Skarlatoudis A.A., Kristek, J., Moczo, P., Papazachos, C.B, 2006. Implementation of a non-splitting formulation of perfect matching layer in a 3D 4th-order staggered-grid velocity-stress finite-difference scheme, in *Proceedings of the 1st European Conference on Earthquake Engineering and Seismology,* Geneva, Switzerland.

Triantafyllidis, P., Hatzidimitriou, P.M, Suhadolc, P., Theodulidis, N. & Pitilakis, K., 1998. Comparison between 1-D and 2-D site effects modelling in Thessaloniki, in *Proceedings of the symposium on Effects of Surface Geology on Seismic Motion,* Yokohama-shi, Japan, 2, pp. 981–986.

Triantafyllidis, P., Hatzidimitriou, P.M, Theodulidis, N., Suhadolc, P., Papazachos, C., Raptakis, D. & Lontzetidis, K., 1999. Site effects in the city of Thessaloniki (Greece) estimated from acceleration data and 1-D local soil profiles, *Bull. seism. Soc. Am., 89,* 521–537.

Triantafyllidis P., Suhadolc, P., Hatzidimitriou, P.M, Anastasiadis, A. & Theodulidis, N., 2004a. Part I. Theoretical site response estimation for microzoning purposes, *Pure appl. Geophys., 161,* 1185–1203.

Triantafyllidis P., Hatzidimitriou, P.M, Suhadolc, P., Theodulidis, N. & Anastasiadis, A., 2004b. Part II. Comparison of theoretical and experimental estimations of site effects, *Pure appl. Geophys., 161,* 1205–1219.

Tsotsos S. & Zissis-Tegos, G., 1986. Seismic microzonation study of Thessaloniki area and comparison with the observed damage distribution during the June, 1978, earthquake, in *Proceedings of the 8th European Conference on Earthquake Engineering,* Lisbon, Portugal.

Vamvakaris D.A., Papazachos C.B., Karagianni E.E., Scordilis E.M. & Hatzidimitriou P.M., 2006. Small-scale spatial variation of the stress field in the back-arc Aegean area: Results from the seismotectonic study of the broader area of Mygdonia basin (N. Greece), *Tectonophysics, 417,* 249–267.

SUPPORTING INFORMATION

Additional Supporting Information may be found in the online version of this article:

Appendix S1. 3-D wave propagation characteristics for scenario 1a.

Please note: Wiley-Blackwell are not responsible for the content or functionality of any supporting materials supplied by the authors. Any queries (other than missing material) should be directed to the corresponding author for the article.